Measurement 211 (2023) 112590

Contents lists available at ScienceDirect

Measurement

journal homepage: www.elsevier.com/locate/measurement

Implementation of Gaussian Process Regression to strain data in residual stress measurements by hole drilling

Claudia Barile, Simone Carone, Caterina Casavola, Giovanni Pappalettera *

Department of Mechanics, Mathematics and Management, Polytechnic University of Bari, Via Orabona n.4, Bari 70125, Italy

ARTICLE INFO

Keywords:
Residual stress
Incremental hole drilling
Gaussian process regression
Machine learning
Laser shock peening
Aluminum alloy

ABSTRACT

Incremental hole drilling is a prominent tool in the surface and sub-surface residual stress measurements. Generally, strains are measured at drilling steps not corresponding to the stress calculation steps of the integral method. Consequently, strain measurements are fitted using polynomials or splines. However, this process is greatly influenced by user's experience, affecting the calculated stresses as an additional source of uncertainty. The present work assesses the uncertainty associated with the strain fitting procedure by exploiting Gaussian Process Regression (GPR), a probabilistic machine learning framework which can yield uncertainties on the fit. These uncertainties were propagated to residual stresses by using Monte Carlo simulation. Laser shock peened AA 7050-T7451 specimens were considered as case study.

The proposed methodology was corroborated by comparing residual stress results with those obtained exploiting traditional fitting procedures and X-ray diffraction measurements. Finally, the GPR-based approach demonstrated its ability to successfully discriminate different strain signal sources.

1. Introduction

Almost every production and manufacturing process gives rise to incompatible local strains of mechanical, chemical or thermal nature, thereby developing a residual stress field in a material or structural component [1,2]. Residual stresses can impact greatly on mechanical properties as for instance distortion, corrosion resistance, brittle fracture and fatigue life [3]. These stresses can be either detrimental and beneficial, however, in both cases a comprehensive assessment of the residual stress state becomes a key factor in engineering design [4,5]. Indeed, tensile residual stresses entail a reduction in the fatigue life of a component, whilst on the other hand a surface compression stress field can enhance fatigue resistance and fracture strength. Therefore, surface treatments such as shot peening and laser shock peening (LSP) have been developed to introduce compressive residual stresses [6,7]. Notably, LSP is increasingly employed in the aeronautical and aerospace industries as it produces deeper compressive residual stresses and has less impact on surface integrity with respect to conventional shot peening [7].

The relevance and the complexity of performing an accurate experimental analysis of the residual stresses within a material has led to the emergence of several measurement techniques. At the present time, incremental hole drilling (IHD) and X-ray diffraction (XRD) are well-established techniques for measuring surface and sub-surface residual stresses and are also ruled by standards[8,9]. XRD technique employs electromagnetic radiation to measure the inter-atomic lattice spacing in crystalline materials [1,10]. A residual stress field deforms this spacing relative to the free-stress state. Therefore, the measured crystal interplanar dimension is related to the magnitude and direction of the residual stress field occurring in the material. In particular, diffraction peaks are shifted from unstressed condition, therefore this shift is used to calculate the residual stress state using solid mechanics formulations [1,10]. On the other hand, stress relief through incremental removal of material and a subsequent measurement of the relaxed strains with the aid of strain gauges is one of the semi-destructive residual stress measurement processes. Material is removed through incremental drilling in the IHD process. Subsequently, when exploiting destructive methods, the measured strains and the residual stresses are related by an integral equation, thus an elastic inverse solution is needed to compute the residual stress field [11,12]. This integral relationship occurs due to the fact that the stresses are calculated in locations different from where released strains are measured. The integral method is by far the predominant calculation method [13–22]. It exploits calibration

* Corresponding author.
E-mail addresses: claudia.barile@poliba.it (C. Barile), simone.carone@poliba.it (S. Carone), caterina.casavola@poliba.it (C. Casavola), giovanni.pappalettera@poliba.it (G. Pappalettera).

https://doi.org/10.1016/j.measurement.2023.112590
Received 17 October 2022; Received in revised form 1 February 2023; Accepted 9 February 2023
Available online 11 February 2023

Nomenclature

D	Dataset of samples
n	Total number of samples
x_i	Depth increments
X	Vector of inputs
$y(x_i)$	Noisy strain measurements
$f(x)$	Unknown strain function
$\in$	Noise in measured strain data
$N(*,*)$	Gaussian distribution
σ_n^2	Variance of the Gaussian distribution
$GP(*,*)$	Gaussian process
$m(x)$	Mean function
$k(x,x')$	Covariance function (kernel function)
f_*	Set of function values corresponding to unseen inputs
X_*	Unseen test set of inputs
$\overline{f_*}$	Mean of the posterior Gaussian process
$cov(f_*)$	Covariance of the posterior Gaussian process
K	Training set covariances
K_*	Training-test set covariances
K_{**}	Test set covariances
I	Identity matrix
k_{SE}	Squared exponential kernel
σ_f	Hyperparameter: vertical scale
l	Hyperparameter: horizontal scale
k_W	White kernel
K_T	Total kernel
θ	Vector of hyperparameters

coefficients, determined by FE calculation and tabulated in ASTM E837-20 [8], which are related to hole diameter, strain gage rosette geometry and drilling depth.

However, the integral method is very sensitive to errors in measured data for two main reasons. The first is physical in nature, as strains are being measured only at the surface. Therefore, IHD is limited by the Saint Venant's Principle, which states that surface deformation response becomes insensitive to the relaxation of residual stresses as hole depth increases. Accordingly, at large hole depths, the difference in measured strains at successive depths becomes progressively smaller, hence the impact of strain measurements errors is amplified [13]. The second reason is related to the numerical instability of the inverse problem. For a high number of calculation steps, the calibration matrices become numerically ill conditioned, so for small errors in the measured strains there are much larger error in the calculated residual stresses [15,16].

Over the past three decades, a number of researchers have investigated the influence of errors on IHD measurements carried out using the integral method. Vangi studied the influence of strain and hole diameter errors on the uncertainties associated to the calculated residual stresses [17]. Schajer and Altus presented a method for estimating probability bounds associated to the computed residual stresses for both the integral and power series methods. In their methodology, they considered the uncertainties related to errors on strains, hole depth, hole diameter and material constants. Then, they identified errors on measured strains as the main source of uncertainty with the largest probability bounds [18]. Zuccarello found that the numerical conditioning of the calibration matrices is minimized by adopting a calculation step distribution in such a way that diagonal elements of the matrices are constant in magnitude. Therefore, strain measurement errors have less effect on residual stress magnitudes and accordingly stress uncertainty is lower [16]. Peral et al. [19] carried out a detailed uncertainty analysis, taking into account many sources of error, performing a Monte Carlo simulation to propagate uncertainties to residual stresses and corroborating results with the more conservative approach proposed by Schajer in [18]. Uncertainty propagation to residual stresses through Monte Carlo simulation was subsequently applied in several other papers, reaffirming that one of the main contributors to uncertainties in stresses was noise in measured strains, especially using the integral method [20,23,24]. Recently, Olson et al. [25] developed an uncertainty estimator that considers two crucial sources of uncertainties. The first is strain uncertainty, where errors arise owing to instrumentation errors, thermally induced strains and residual stresses induced by the drilling process itself [12,18]. Whereas the second uncertainty source originates from the selection of the regularization parameters, which can significantly influence the calculated stresses.

Nevertheless, another source of uncertainty associated with the numerical manipulation of experimentally measured strain data should be considered. Generally, the drilling steps where the strains are measured do not match the calculation steps of the integral method. Therefore, Vangi proposed to interpolate the measured or the transformed strains using a polynomial, such that the maximum deviation from experimental values is lower than the measurement error [17]. Thus, it is now common practice to smooth the strain data using a polynomial or a spline [20–23,26–29]. However, this process is hugely influenced by the user's experience in choosing the degree of the fitting polynomial or the amount of smoothing given by the spline. Consequently, the fit procedure has an impact on the calculated residual stresses due to the sensitivity of the integral method.

In this research investigation, a tool based on the Gaussian Process Regression (GPR) is implemented to assess the uncertainty associated with the strain fitting procedure [30]. A Gaussian process model is a probabilistic supervised machine learning framework, which provides uncertainty measures over the predictions. It describes a probability distribution over possible functions that fit a dataset, by assuming that these functions are jointly Gaussian distributed [31]. GPR is an emerging framework among machine learning practitioners, nonetheless it has also recently been applied in the field of experimental mechanics by Tognan et al. to model the uncertainty over the residual stresses when employing the contour method [32].

The present work is focused on developing a methodology to quantify the strain uncertainty in IHD, taking into account the uncertainty associated to strain fitting. Moreover, strain uncertainties were propagated to the calculated residual stresses by exploiting Monte Carlo simulation [33]. To validate this methodology a laser shock peened AA 7050-T7451 specimen was considered as case study [34]. Furthermore, the results were compared to those obtained using traditional polynomial fitting procedures and also to XRD measurements on an analogous sample. Finally, the ability of the proposed probabilistic method to discriminate two different strain signal sources was investigated.

2. Materials and methods

2.1. Specimen and laser shock peening

Squared samples 65 mm × 65 mm of aluminum alloy 7050-T7451 were machined from a rolled plate with a thickness of 30 mm. To achieve T7451 temper, the metal is solution heat-treated, stress relieved by controlled stretching and then stabilized by artificial overaging. The chemical composition and the mechanical properties of the material are given in Table 1 and Table 2, respectively. Prior to laser shock peening, the surface to be processed was ground. The LSP samples were realized using a YLF:Nd laser, the specification of which are reported in Table 3. The treatment was applied to an area of 35 mm × 35 mm placed in the middle of upper face of the specimens, as can be seen in Fig. 1a. Surfaces

Table 1
Chemical composition (wt%) of aluminum alloy 7050-T7451 [35].

Al	Cr	Cu	Fe	Mg	Mn	Si	Ti	Zn	Zr	Others
87.3 – 90.3	≤0.04	2.0 – 2.6	≤0.15	1.9 – 2.6	≤0.10	≤0.12	≤0.06	5.7 – 6.7	0.08 – 0.15	≤0.15

Table 2
Mechanical properties of aluminum alloy 7050-T7451 [35].

Young's Modulus (GPa)	Poisson's ratio	Yield strength (MPa)	Ultimate tensile strength (MPa)
71.7	0.33	469	524

of the samples were laser shock peened setting the pulse frequency to 5 Hz, using a spot diameter of 3.5 mm attaining a nominal power density of 4.5 GW/cm^2. Prior to the peening process, a 30–40 μm thick commercial black paint layer and a film of 2 mm distilled water are used, respectively, as the sacrificial adhesive coating layer and the transparent confining layer. The sacrificial layer is limited to the surfaces of the treated areas only. An X-Y raster pattern was used as the peening strategy, where the LSP scan and step directions correspond to the x and y directions, respectively (Fig. 1b). In the LSP process, an overlap of 30 percent was set between two adjacent laser spots, both along the scan and the step directions. Furthermore, 3 layers of peening were performed and an offset of 33 percent of a spot diameter was imposed between two consecutive layers.

2.2. Experimental set-up for incremental hole drilling measurements

IHD was performed using the Sint Technology Hole Drilling system Restan MTS 3000 equipped with a compressed air unit controlling a pneumatic turbine which achieves a rotation speed of 400,000 rpm. The strain evolutions during the IHD process are measured using a type B counterclockwise strain gauge rosette. This was installed in the center of the surface treated area, such that the "a" and the "c" grids were aligned to the LSP scan and step directions, respectively. The roughness, introduced by the LSP process, was evaluated within the limits specified by the rosette manufacturer for proper installation of the strain gauge rosette. TiAlN coated tungsten carbide with higher durability and toughness was used as the mill. The inverted cone end mill of 1.6 mm diameter was employed to cut the hole, which had a precise final diameter of 1.98 mm. A total of 20 drilling steps with a polynomial distribution were executed at a speed of 0.2 mm/min to attain a final hole depth of 1 mm. The IHD experimental set-up is shown in Fig. 2.

2.3. Gaussian process regression and propagation of uncertainties

As already mentioned above, a GPR model can make predictions on input data and deliver measurements of uncertainty on those predictions. In IHD strain fitting, the incremental drilling depths can be considered as input training data, whereas the output are the measured strains by the three strain gauges. Given a dataset $D = \{(x_i, y(x_i), i \in \{1, \cdots, n\})\}$, where n is the total number of samples in the dataset, x_i are the depth increments that can be aggregated in a vector of inputs X, and $y(x_i)$ are the noisy strain measurements of an unknown function $f(x)$ sampled at x_i. The measured strains $y(x_i)$ can be modelled as follows:

$$y(x_i) = f(x_i) + \epsilon, \quad \epsilon \sim N\left(0, \ \sigma_n^2\right) \tag{1}$$

where $\epsilon \sim N(0, \sigma_n^2)$ is the noise in the measured strain data, which is modelled as a Gaussian distribution with zero mean and variance σ_n^2. A GPR is defined as a random distribution of functions such that any finite samples of functions have a joint Gaussian distribution [30]. A Gaussian process is completely specified by its mean function $m(x)$ and its covariance function $k(x, x')$, also called kernel function:

$$f \sim GP(m(x), k(x, x')) \tag{2}$$

Therefore in GPRs there is the possibility to explicitly model a mean

Table 3
Laser specifications.

Laser source	Wavelength (nm)	Laser power (W)	Pulse energy range (J)	Pulse length range (nm)	Pulse frequency range (Hz)	Beam shape	Beam profile	Spot diameter range (mm)
YLF:Nd	1053	200	Up to 10	16 – 21	1 – 20	Round	Flattop	2 – 6

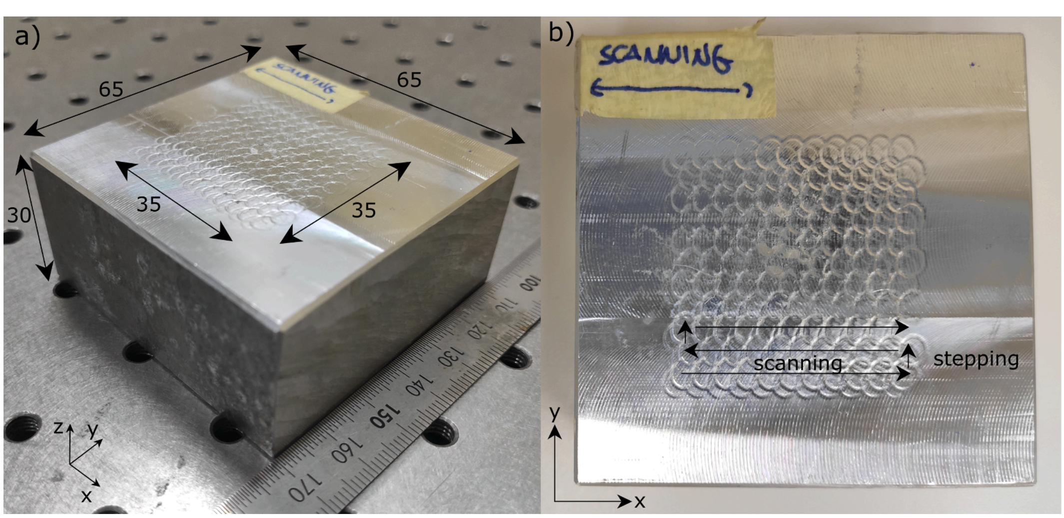

Fig. 1. a) LSP samples dimensions; b) LSP scanning strategy. All dimensions are in mm.

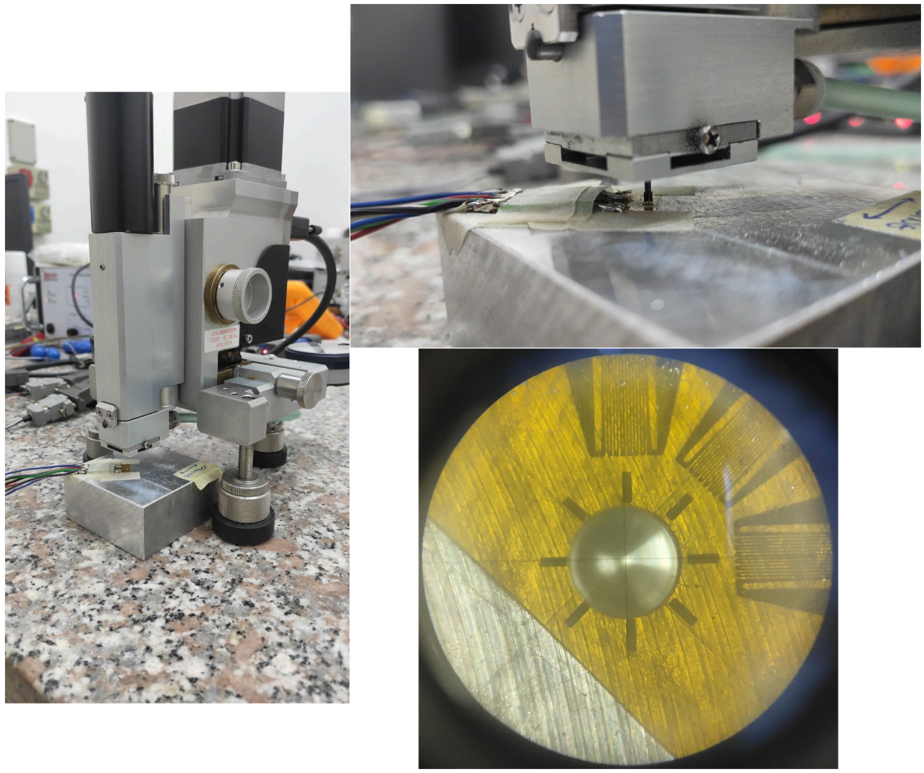

Fig. 2. Incremental Hole Drilling set-up.

function, which can offer advantages such as interpretability of the model, convenience of expressing prior information and analytical limitations. However, if no prior information is available, it is common to set the mean function $m(x) = 0$, considering that this is not a drastic limitation, since the mean of the posterior process is not constrained to be zero [30]. In GPR models, after selecting the prior mean and covariance, this prior information is updated in light of the training data by defining the posterior, which is used to make predictions on unseen data.

Considering the case in which the mean function of the GP is zero and that the y observations are affected by noise (equation **(1)**), in order to make predictions we need to compute the conditional probability distribution of f_* given y, where f_* is a set of function values corresponding to new unseen test set of inputs X_*. Exploiting the closure property of Gaussians, we obtain that the conditional distribution is still Gaussian. This is called posterior GP, having mean and variance given by:

$$\overline{f_*} = K_*^T\left[K + \sigma_n^2 I\right]^{-1} y \tag{3}$$

$$cov(f_*) = K_{**} - K_*^T\left[K + \sigma_n^2 I\right]^{-1} K_* \tag{4}$$

where K refers to training set covariances, K_* refers to training-test set covariances, K_{**} refers to test set covariances and I is the identity matrix. It can be noted that $cov(f_*)$ models the uncertainty regarding the predictions at X_*. Besides, the confidence intervals on the GPR predictions can also be obtained through this.

In this research investigation, the kernel function used to model the GPR is the radial basis function, also known as squared exponential kernel:

$$k_{SE}(x_i, x_j) = \sigma_f^2 \exp\left(-\frac{(x_i - x_j)^T (x_i - x_j)}{2l}\right) \tag{5}$$

where σ_f and l are hyperparameters. The vertical scale σ_f represents the vertical span of the function f, whereas, the horizontal scale l describes the correlation between the points x_i and x_j as a result of the decrease in their distances. The squared exponential kernel is broadly used and is a universal approximator, capable of approximating any arbitrary continuous function on any compact set of the input space [36].

In this work, since the additive noise ϵ present in the measured data depends on various factors as for instance instrumentation errors, thermally induced strains and residual stresses induced by the drilling process, the noise variance σ_n^2 was estimated by adding to the squared exponential kernel a white kernel [37]. It makes the assumption that the noise in the signal is independent and identically normally distributed, and it is defined as follows:

$$k_W(x_i, x_j) = \sigma_n^2 I \tag{6}$$

where σ_n^2 is the variance of the noise and I is the identity matrix. Therefore σ_n is another hyperparameter. Then we can define the total kernel function used as $K_T = k_{SE} + k_W$ and we can collect the hyperparameters in a column vector $\theta = [\sigma_f, l, \sigma_n]$.

The optimal hyperparameters are automatically determined by maximizing the log marginal likelihood [30]:

$$\log p(y|X, \theta) = -\frac{1}{2} y^T K_T^{-1} y - \frac{1}{2}\log|K_T| - \frac{n}{2}\log 2\pi \tag{7}$$

The GPR algorithm was implemented using the Python module scikit-learn [38]. To facilitate the search for optimal hyperparameters, the input dataset of depth increments and measured strains was given with measurement units of mm and $m\epsilon$, respectively. The optimal hyperparameters are reported in Table 4.

Afterwards, by exploiting the posterior GPR, the strains were predicted for 20 linear depth increments corresponding to the calculation

Table 4
Optimal hyperparameters.

σ_f	l	σ_n
537 $\mu\epsilon$	0.529 mm	5.594 $\mu\epsilon$

steps of the integral method for a hole 1 mm deep. Then the residual stress magnitudes were calculated following [8], without additional Tikhonov regularization. The GPR uncertainties, associated with each calculation depth, of the three strain measurements were propagated to the residual stress magnitudes through the use of Monte Carlo simulations [33]. Ten thousand trials were simulated, where for each trial the strain values were randomly drawn from the specific uncertainty distributions of each calculation depth.

2.4. Validation of the proposed method

To validate the proposed methodology, GPR residual stresses were compared with conventional approaches exploiting the integral method, in particular: results obtained by a strain fitting 4th degree polynomial; residual stresses derived from a 12th degree polynomial which minimized the residuals between the fit and the measured strains, which is the degree of smoothing suggested by the Sint Technology commercial software; residual stresses measured by XRD on an analogous specimen conducted in [34].

Furthermore, to verify the ability of the proposed method to discriminate two different IHD measurements, two new sets of data were created by adding normal random noise with zero mean to the original strain measurements given by the three strain gauges. Then residual stress magnitudes were evaluated by exploiting GPR. First, a Gaussian noise with a standard deviation of 5 με was added, representing a signal within the strain measurement error. Secondly, a Gaussian noise with a 15 με standard deviation was added to the original data, representing an IHD measurement outside of the strain measurement error and that should lie outside of residual stress uncertainty bounds.

3. Results and discussions

Fig. 3 shows the strain measurements by the three strain gauges. Whereas, Fig. 4 illustrates the GPR predictions over the measured strain data along with the associated uncertainties, reported with a confidence level of 99.7% for visual clarity.

Table 5 reports the mean, minimum and maximum values of the uncertainties estimated by the GPR. It can be seen that the average uncertainty value between the three strain gauges is around 6 με. Furthermore, the minimum values of uncertainty, which are very close to the respective averages, for all the measured strains are located in the range of 0.1 to 0.85 mm of depth. Conversely, higher uncertainty values occur at the surface and the maximum is always found at depths greater than 0.85 mm. This could be attributed to the smaller number of measured strain data present in these two regions. Indeed, due to the polynomial distribution of the drilling depth increments, as the depth increases, the drilling step becomes larger, thus there are less measured strains in the deepest region of the hole. Therefore, in Fig. 4 can be seen that GPR successfully fitted the outer data but with higher uncertainty.

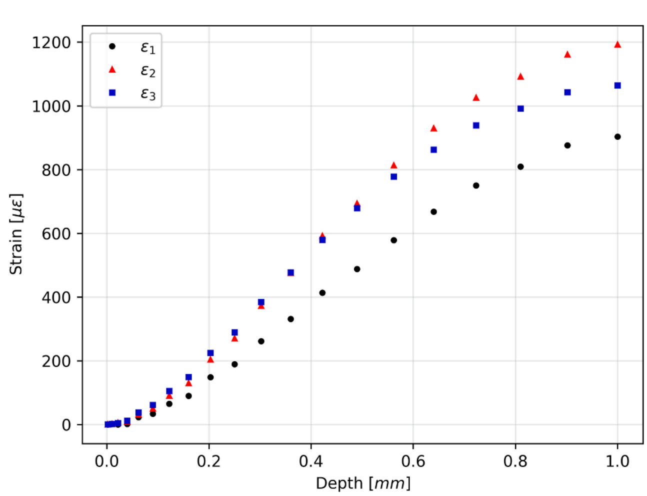

Fig. 3. Measured strain variation with depth in the three strain gauges directions.

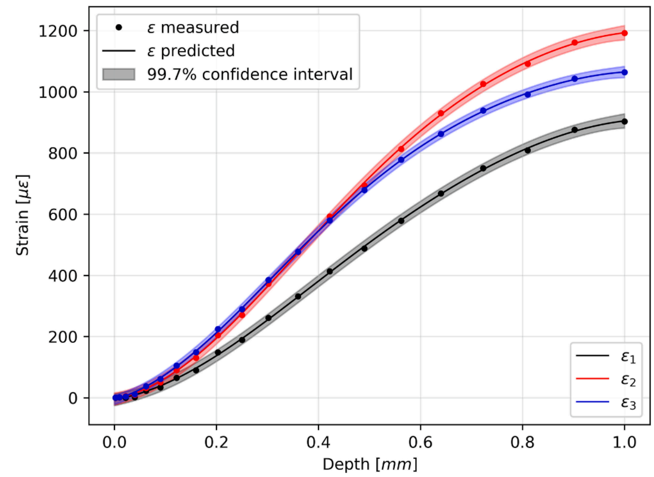

Fig. 4. GPR fit of the measured strain data, with associated uncertainties shown as ± 3σ.

Thereafter, the strain uncertainties were propagated to residual stresses through Monte Carlo simulations. Fig. 5 depicts residual stresses along scan and step directions, denoted as σ_x and σ_y, respectively. Stress uncertainties are reported with a confidence level of 68%. Fig. 5 shows that an X-Y raster peening strategy induced compressive residual stresses which are slightly different in the two directions, especially for the first 0.4 mm from surface. Indeed, the compression along the step direction is greater than in the scan direction, reaching – 400 MPa at 0.3 mm deep. This behavior is also reported in [21] and by Correa et al. in [39], where it was found that residual stress magnitudes exhibit differences in perpendicular directions in LSP samples peened using a raster strategy, compared to those induced by adopting a random LSP pattern strategy. Furthermore, as can be seen in Fig. 5, for both stress components, between 0.15 mm and 0.85 mm depth the uncertainty is below 19 MPa, notably in the middle depth range it reaches a minimum of 5 MPa. On the other hand, at the surface the uncertainty increases due to the higher strain uncertainty. As mentioned earlier, the strain uncertainty also takes into account errors related to the drilling process and, more generally, the strain measurement process, which are particularly critical at the surface. For this reason, a greater uncertainty on stresses is observed at surface [12,18,25]. In addition, in the deeper region of the hole, stress uncertainty increases significantly due to a combination of factors. Since twenty calculation steps are used, this uncertainty increase is due to the ill conditioning of the inverse problem in the integral method and is exacerbated by higher strain uncertainty detected by the GPR. Furthermore, as shown in Fig. 5, in the depth region between 0.275 mm and 0.425 mm, the magnitude of residual stresses along step direction σ_y exceeds the ASTM limit of 80% of the material yield strength, under which plasticity effects around the hole are prevented [8]. The correction procedure to include the effect of plasticity reported in [40] was applied, under the conservative assumptions of uniform residual stresses equal to the maximum σ_y, at a greater depth of 0.51 mm. The plasticity effect was found to be below 2 percent, therefore it can be neglected [40].

Figs. 6 and 7 show comparisons of residual stresses measured by using: GPR methodology; a 4th degree fitting polynomial; a 12th degree fitting polynomial which minimized residuals; XRD [34]. The XRD results in [34] go down to 2.5 mm depth, but in Figs. 6 and 7 they are reported at the same depth as IHD measurements for visual clarity. XRD measurements, up to the depth of 1 mm, exhibit maximum errors in the scan and step directions equal to ± 34.1 MPa and ± 35 MPa,

Table 5
Mean, minimum and maximum values of uncertainties estimated by the GPR.

Mean σ_{ϵ_1} ($\mu\epsilon$)	Mean σ_{ϵ_2} ($\mu\epsilon$)	Mean σ_{ϵ_3} ($\mu\epsilon$)	Min σ_{ϵ_1} ($\mu\epsilon$)	Min σ_{ϵ_2} ($\mu\epsilon$)	Min σ_{ϵ_3} ($\mu\epsilon$)	Max σ_{ϵ_1} ($\mu\epsilon$)	Max σ_{ϵ_2} ($\mu\epsilon$)	Max σ_{ϵ_3} ($\mu\epsilon$)
6	6	5	6	6	5	8	8	6

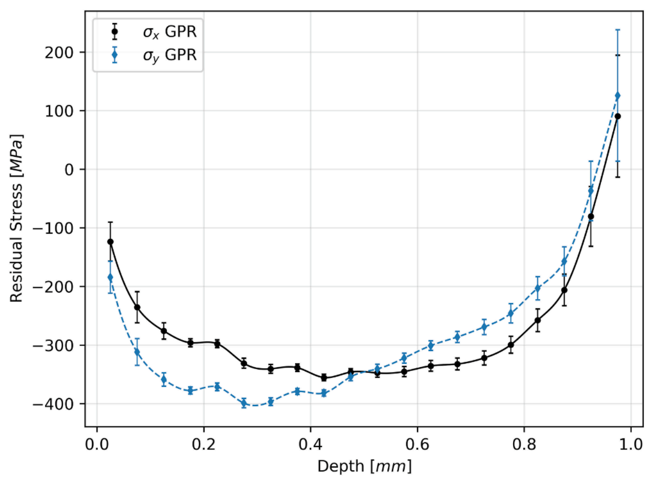

Fig. 5. Residual stress distribution in scan (x) and step (y) directions, calculated using GPR, with propagated stress uncertainties shown as ± 1σ.

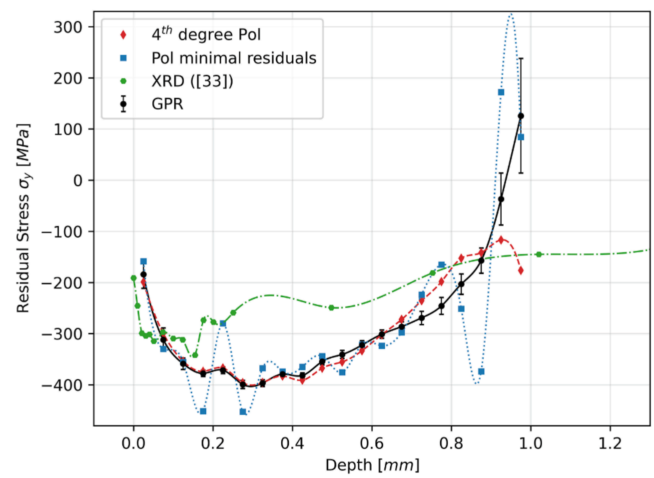

Fig. 7. Comparison of residual stresses in step (y) direction obtained by GPR method, by a 4th degree fitting polynomial, by a fitting polynomial of 12th degree which minimized the residuals, and by XRD [34].

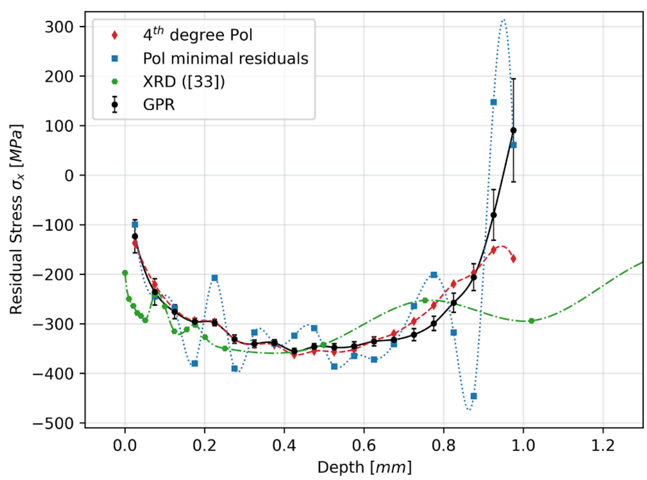

Fig. 6. Comparison of residual stresses in scan (x) direction obtained by GPR method, by a 4th degree fitting polynomial, by a fitting polynomial of 12th degree which minimized the residuals, and by XRD [34].

respectively [34]. It can be seen that, for both residual stress components, GPR results are smooth and do not need additional regularization. Conversely, using the higher degree polynomial, which minimized residuals, residual stress magnitudes exhibit a highly oscillating behavior and always lay outside of GPR uncertainty boundaries. Furthermore, the 4th degree fitting polynomial is in good agreement with GPR results, indeed it falls within uncertainty limits until 0.675 mm deep. Fig. 6 shows an excellent agreement between GPR and XRD measurements with a maximum difference of less than 80 MPa until a depth of 0.875 mm. Conversely, in Fig. 7 residual stresses along step direction measured by XRD exhibit a decrease of compression from 0.175 mm, increasing the difference with IHD measurements. However, an overall agreement occurs between the two different measurement methods, which further corroborates the GPR methodology, especially in the scan direction.

Figs. 8 and 9 illustrate the ability of the GPR methodology to correctly discriminate two different strain signal sources. They show residual stresses in scan and step directions, respectively. On the one hand, the original strain signal with an added Gaussian noise with zero mean and a standard deviation of 5 με correctly lies within stress uncertainty bounds given by the GPR method. On the other hand, the strain signal with a noise of 15 με standard deviation falls outside of the uncertainty limits for almost every calculation step. Therefore, the GPR method properly identifies a strain signal that is within the strain measurement error as equal to the original strain signal, and correctly discriminate a strain signal that exceed this limit as different. Consequently, the GPR based approach does not introduce a level of smoothing that distorts the underlying stress solution, but successfully discriminate between different solutions.

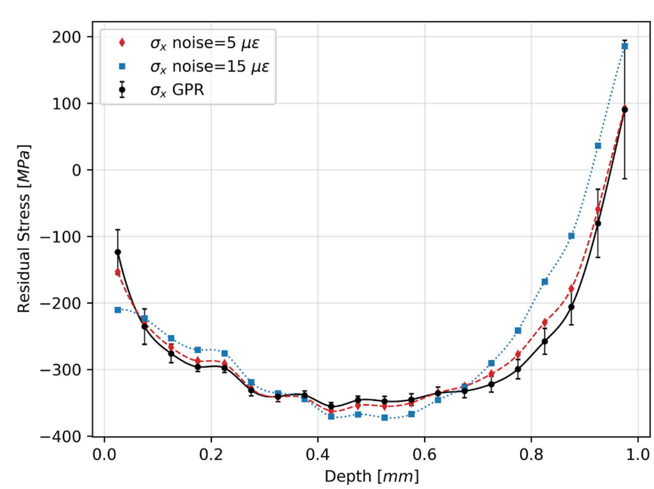

Fig. 8. Comparison of GPR residual stresses in scan (x) direction with two different strain signal sources with Gaussian additive noise of 5 με and 15 με standard deviations.

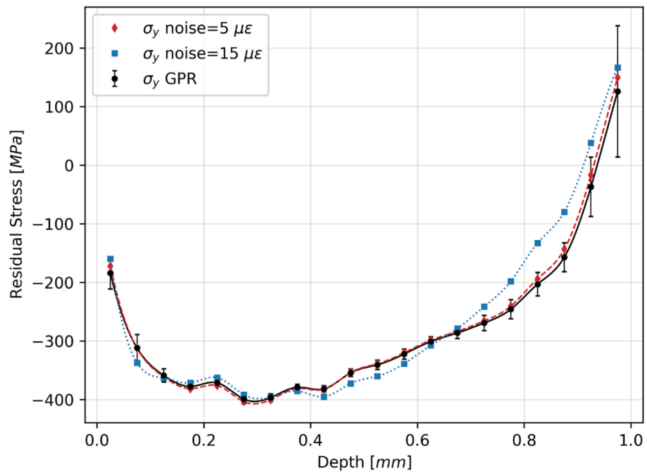

Fig. 9. Comparison of GPR residual stresses in step (y) direction with two different strain signal sources with Gaussian additive noise of 5 με and 15 με standard deviations.

4. Conclusions

Generally, in IHD measurements with integral approach the drilling steps where strains are measured do not correspond to the stress calculation steps. Therefore, practitioners perform a fit of strain measurements using polynomials or splines introducing a source of uncertainty, associated with this fitting procedure (e.g. degree of polynomial or spline parameters), to the calculated stresses.

In this research work, a tool based on GPR was developed, which served two purposes. One is to fit the experimental strains during the IHD process and two is to estimate the uncertainties arising from this procedure. Moreover, GPR has the advantage that the optimal hyperparameters are automatically determined by maximizing the log marginal likelihood. Hence, the user's influence on the calculated residual stresses is minimized. Furthermore, GPR not only inferred uncertainty related to the fitting procedure, but also incorporated error sources connected to strain measurement procedure, e.g. instrumentation errors and drilling induced strains, by exploiting a compound kernel consisting of a squared exponential and a white kernel. In addition, a Monte Carlo simulation was carried out in order to propagate GPR uncertainties to the calculated residual stresses.

The GPR proposed methodology successfully fitted strain data of a laser shock peened AA 7050-T7451 specimen. From 0.15 mm to 0.85 mm deep residual stress magnitudes reported uncertainties between 5 MPa and 19 MPa. At the surface results exhibited a slightly higher level of uncertainty, whereas in the deeper region of the hole stress uncertainties significantly increased both owing to higher strain uncertainty and to the ill conditioning of the inverse problem.

To corroborate the proposed methodology, the obtained residual stress magnitudes were compared to traditional polynomial fitting procedures for both scan and step directions. The GPR-based approach yielded smooth residual stress results without the need for further regularization. In addition, results were consistent with XRD measurements on a similar specimen, especially along scan direction.

Finally, the proposed method demonstrated its ability to successfully discriminate between different strain signal sources that yield different stress solutions.

Funding

This research did not receive any specific grant from funding agencies in the public, commercial, or not-for-profit sectors.

CRediT authorship contribution statement

Claudia Barile: Conceptualization, Methodology, Investigation, Writing – review & editing, Supervision. **Simone Carone:** Conceptualization, Methodology, Software, Formal analysis, Investigation, Data curation, Writing – original draft, Visualization. **Caterina Casavola:** Project administration, Funding acquisition. **Giovanni Pappalettera:** Conceptualization, Methodology, Writing – review & editing, Supervision.

Declaration of Competing Interest

The authors declare that they have no known competing financial interests or personal relationships that could have appeared to influence the work reported in this paper.

Data availability

Data will be made available on request.

References

[1] G.S. Schajer, C.O. Ruud, Overview of residual stresses and their measurement, in: Pract. Residual Stress Meas. Methods, 2013: pp. 1–27.
[2] P.J. Withers, H. Bhadeshia, Residual stress. Part 2–Nature and origins, Mater. Sci. Technol. 17 (2001) 366–375, https://doi.org/10.1179/026708301101510087.
[3] N.S. Rossini, M. Dassisti, K.Y. Benyounis, A.G. Olabi, Methods of measuring residual stresses in components, Mater. Des. 35 (2012) 572–588, https://doi.org/10.1016/j.matdes.2011.08.022.
[4] C. Casavola, C. Barile, V. Moramarco, G. Pappalettera, Introductory Chapter: New Challenges in Residual Stress Measurements and Evaluation, in: New Challenges Residual Stress Meas. Eval., 2020: pp. 1–4. https://doi.org/10.5772/intechopen.92620.
[5] C. Barile, C. Casavola, G. Pappalettera, C. Pappalettere, Remarks on residual stress measurement by hole-drilling and electronic speckle pattern interferometry, Sci. World J. (2014), https://doi.org/10.1155/2014/487149.
[6] G.A. Webster, A.N. Ezeilo, Residual stress distributions and their influence on fatigue lifetimes, Int. J. Fatigue. 23 (2001) 375–383, https://doi.org/10.1016/s0142-1123(01)00133-5.
[7] C.S. Montross, T. Wei, L. Ye, G. Clark, Y.W. Mai, Laser shock processing and its effects on microstructure and properties of metal alloys: A review, Int. J. Fatigue. 24 (2002) 1021–1036, https://doi.org/10.1016/S0142-1123(02)00022-1.
[8] ASTM E837-20, Standard Test Method for Determining Residual Stresses by the Hole-Drilling Strain-Gage Method, ASTM International, West Conshohocken, PA., (2020).
[9] European Committee for Standardization EN 15305:2008 E, Non-destructive Testing – Test Method for Residual Stress analysis by X-ray Diffraction, (2008).
[10] C.E. Murray, I.C. Noyan, Applied and Residual Stress Determination Using X-ray Diffraction, in: G.S. Schajer (Ed.), Pract. Residual Stress Meas. Methods, First Edit, John Wiley & Sons Ltd, Hoboken, NJ, USA, 2013, pp. 139–161.
[11] G.S. Schajer, M.B. Prime, Use of inverse solutions for residual stress measurements, J. Eng. Mater. Technol. 128 (2006) 375–382, https://doi.org/10.1115/1.2204952.
[12] M.B. Prime, M.R. Hill, Uncertainty, model error, and order selection for series-expanded, residual-stress inverse solutions, J. Eng. Mater. Technol. 128 (2006) 175–185, https://doi.org/10.1115/1.2172278.
[13] G.S. Schajer, Measurement of Non-Uniform Residual Stresses Using the Hole-Drilling Method. Part I—Stress Calculation Procedures, J. Eng. Mater. Technol. 110 (1988) 338–343, https://doi.org/10.1115/1.3226059.
[14] G.S. Schajer, Measurement of Non-Uniform Residual Stresses Using the Hole-Drilling Method. Part II—Practical Application of the Integral Method, J. Eng. Mater. Technol. 110 (1988) 344–349, https://doi.org/10.1115/1.3226060.
[15] G.S. Schajer, Hole-drilling residual stress profiling with automated smoothing, J. Eng. Mater. Technol. 129 (2007) 440–445, https://doi.org/10.1115/1.2744416.
[16] B. Zuccarello, Optimal calculation steps for the evaluation of residual stress by the incremental hole-drilling method, Exp. Mech. 39 (1999) 117–124, https://doi.org/10.1007/BF02331114.
[17] D. Vangi, Data management for the evaluation of residual stresses by the incremental hole-drilling method, J. Eng. Mater. Technol. Trans. ASME. 116 (1994) 561–566, https://doi.org/10.1115/1.2904329.
[18] G.S. Schajer, E. Altus, Stress calculation error analysis for incremental hole-drilling residual stress measurements, J. Eng. Mater. Technol. Trans. ASME. 118 (1996) 120–126, https://doi.org/10.1115/1.2805924.
[19] D. Peral, J. de Vicente, J.A. Porro, J.L. Ocaña, Uncertainty analysis for non-uniform residual stresses determined by the hole drilling strain gauge method, Meas. J. Int. Meas. Confed. 97 (2017) 51–63, https://doi.org/10.1016/j.measurement.2016.11.010.
[20] T.C. Smit, R.G. Reid, Tikhonov regularization with Incremental Hole-Drilling and the Integral Method in Cross-Ply Composite Laminates, Exp. Mech. 60 (2020) 1135–1148, https://doi.org/10.1007/s11340-020-00629-x.

[21] J.P. Nobre, C. Polese, S.N. van Staden, Incremental Hole Drilling Residual Stress Measurement in Thin Aluminum Alloy Plates Subjected to Laser Shock Peening, Exp. Mech. 60 (2020) 553–564, https://doi.org/10.1007/s11340-020-00586-5.
[22] T.C. Smit, R.G. Reid, Imposition of Constraints on the Regularized Integral Method of Incremental Hole-Drilling, Exp. Mech. (2022), https://doi.org/10.1007/s11340-022-00851-9.
[23] T.C. Smit, R.G. Reid, Residual Stress Measurement in Composite Laminates Using Incremental Hole-Drilling with Power Series, Exp. Mech. 58 (2018) 1221–1235, https://doi.org/10.1007/s11340-018-0403-6.
[24] T.C. Smit, R.G. Reid, Use of Power Series Expansion for Residual Stress Determination by the Incremental Hole-Drilling Technique, Exp. Mech. 60 (2020) 1301–1314, https://doi.org/10.1007/s11340-020-00642-0.
[25] M.D. Olson, A.T. DeWald, M.R. Hill, Precision of Hole-Drilling Residual Stress Depth Profile Measurements and an Updated Uncertainty Estimator, Exp. Mech. 61 (2021) 549–564, https://doi.org/10.1007/s11340-020-00679-1.
[26] C. Cellard, D. Retraint, M. François, E. Rouhaud, D. Le Saunier, Laser shock peening of Ti-17 titanium alloy: Influence of process parameters, Mater. Sci. Eng. A. 532 (2012) 362–372, https://doi.org/10.1016/j.msea.2011.10.104.
[27] U. Trdan, J.A. Porro, J.L. Ocaña, J. Grum, Laser shock peening without absorbent coating (LSPwC) effect on 3D surface topography and mechanical properties of 6082–T651 Al alloy, Surf. Coatings Technol. 208 (2012) 109–116, https://doi.org/10.1016/j.surfcoat.2012.08.048.
[28] M.R. Viotti, A. Albertazzi, Approximated Repair Methods for Outlier Strain Data from Hole-Drilling Residual Measurements, Exp. Mech. 53 (2013) 393–403, https://doi.org/10.1007/s11340-012-9642-0.
[29] B. Gore, J.P. Nobre, Effects of Numerical Methods on Residual Stress Evaluation by the Incremental Hole-Drilling Technique Using the Integral Method, Mater. Res. Proc. 2 (2017) 587–592, https://doi.org/10.21741/9781945291173-99.
[30] C.E. Rasmussen, C.K.I. Williams, Gaussian processes for machine learning, The MIT Press, 2006.
[31] J. Wang, An Intuitive Tutorial to Gaussian Processes Regression, (2020). https://doi.org/http://arxiv.org/abs/2009.10862.
[32] A. Tognan, L. Laurenti, E. Salvati, Contour Method with Uncertainty Quantification: A Robust and Optimised Framework via Gaussian Process Regression, Exp. Mech. (2022), https://doi.org/10.1007/s11340-022-00842-w.
[33] JCGM 101:2008 Supplement 1 – Propagation of distributions using a Monte Carlo method, 1 (2008) 90.
[34] M.A. Attolico, C. Barile, C. Casavola, V. Moramarco, D. Furfari, D.O. Busse, Effects of Laser Shock Peening on Surface Roughness and Residual Stress of AA 7050–T7451, J. Mater. Eng. Perform. (2022), https://doi.org/10.1007/s11665-022-06857-7.
[35] Metals Handbook, Vol.2 - Properties and Selection: Nonferrous Alloys and Special-Purpose Materials, ASM International, 1990.
[36] C.A. Micchelli, Y. Xu, H. Zhang, Universal kernels, J. Mach. Learn. Res. 7 (2006) 2651–2667.
[37] D.K. Duvenaud, Automatic Model Construction with Gaussian Processes, University of Cambridge, 2014.
[38] F. Pedregosa, G. Varoquaux, A. Gramfort, V. Michel, B. Thirion, 0. Grisel, M. Blondel, P. Prettenhofer, R. Weiss, V. Dubourg, J. Vanderplas, A. Passos, D. Cournapeau, M. Brucher, M. Perrot, E. Duchesnay, Scikitlearn: machine learning in python, J. Mach. Learn. Res. 12 (2011) 2825–2830.
[39] C. Correa, D. Peral, J.A. Porro, M. Díaz, L. Ruiz De Lara, A. García-Beltrán, J. L. Ocaña, Random-type scanning patterns in laser shock peening without absorbing coating in 2024–T351 Al alloy: A solution to reduce residual stress anisotropy, Opt. Laser Technol. 73 (2015) 179–187, https://doi.org/10.1016/j.optlastec.2015.04.027.
[40] M. Beghini, L. Bertini, C. Santus, A procedure for evaluating high residual stresses using the blind hole drilling method, including the effect of plasticity, J. Strain Anal. Eng. Des. 45 (2010) 301–318, https://doi.org/10.1243/03093247JSA579.